

Coal fly ash supported nZnO for the sorption of triphenyltin chloride

Olushola S. Ayanda^{1*}, Olalekan S. Fatoki², Folahan A. Adekola³, Bhekumusa J. Ximba²,
Olatunbosun S. Akinsoji², Leslie F. Petrik⁴

¹Federal University Oye Ekiti, Nigeria

Department of Industrial Chemistry

²Cape Peninsula University of Technology, South Africa

Faculty of Applied Sciences

Department of Chemistry

³University of Ilorin, Nigeria

Department of Chemistry

⁴University of the Western Cape, South Africa

Department of Chemistry

*Corresponding author's e-mail: osayanda@gmail.com

Keywords: organotin compounds, triphenyltin, coal fly ash, nZnO, composite, marine, shipyard process wastewater, seawater, adsorption.

Abstract: A laboratory study was performed to study the effects of various operating factors, *viz.* adsorbent dose, contact time, solution pH, stirring speed, initial concentration and temperature on the adsorption of triphenyltin chloride (TPT) onto coal fly ash supported nZnO (CFAZ). The adsorption capacity increases with increase in the adsorbent amount, contact time, pH, stirring speed and initial TPT concentration, and decrease with increase in the solution temperature. The adsorption data have been analyzed by Langmuir, Freundlich, Temkin and Dubinin-Radushkevich (D-R) adsorption models to determine the mechanistic parameters associated with the adsorption process while the kinetic data were analyzed by pseudo first-order, pseudo second-order, Elovich, fractional power and intraparticle diffusivity kinetic models. The thermodynamic parameters of the process were also determined. The results of this study show that 0.5 g of CFAZ was able to remove up to 99.60% of TPT from contaminated natural seawater at 60 min contact time, stirring speed of 200 rpm and at a pH of 8. It was also found that the equilibrium and kinetic data fitted better to Freundlich and pseudo second-order models, respectively. It can therefore be concluded that CFAZ can be effectively used for shipyard process wastewater treatment.

Introduction

Coal fly ash (CFA) is a by-product of the combustion of pulverized coal in electric power generating plants. It consists of fine, powdery particles that are spherical in shape, and mostly glassy in nature. At present, CFA is used in the cement and concrete building industry, but is still largely disposed in landfills and in the filling of dams and lagoons (Querol et al. 2002). With only about 20–30% of the generated CFA being used as additive in cement and concrete manufacture, the management of CFA consequently becomes a global concern from the environmental and economic points of view (Wang, 2008). CFA consists of crystalline aluminosilicate, mullite and α -quartz along with trace amounts of calcium, magnesium, potassium, sodium and titanium oxides, depending on the nature of the coal burned. The particle size distribution patterns of the spherically shaped CFA are in the range of 1–100 μm based on the processing conditions (Nath et al. 2010a, Nath et al. 2010b).

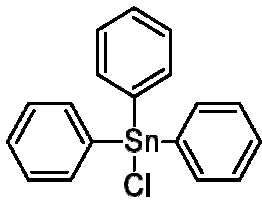
Owing to the high silica and alumina content, CFA can be converted into zeolite-like crystalline materials by chemical treatment, and would find use as adsorbents and ion exchangers in water and wastewater treatment (Juan et al. 2002, Penilla et al. 2006). Rohatgi et al. 2006 reported the application of CFA as composites in reinforced glass and polymer matrix, composites with metals while Wang, 2008 and Dunens et al. 2009 reported its application as catalyst supports. The application of CFA for the remediation of environmental pollutants has also been widely reported (Papandreou et al. 2007, Wang et al. 2008, Nascimento et al. 2009, Wei et al. 2011) but the surface area of CFA is exceptionally low (Ayanda et al. 2012a). Hence, there is a need to improve the surface area and porosity of CFA to enhance its adsorption capacity.

Nano oxides such as nFe⁰, nZnO, nFe₃O₄ etc. have great potential in a wide array of environmental applications such as soil, sediment and wastewater remediation (Poursaberi et al. 2012) due to their extremely small particle size and large surface area. Thus, nano zinc oxide (nZnO) has been studied

as potential adsorbent of dyes (organic compound) by many authors (Zhang et al. 2008, Ada et al. 2009, Salehi et al. 2010), Yue et al. 2011 also reported the removal of methylene blue dye by exfoliated graphite/ZnO composites. However, reports on the adsorption capacity of endocrine disrupting chemicals (ECD) onto nZnO and composites of nZnO are still very rare. Application of coal fly ash supported with nZnO (CFAZ) can result with physicochemical properties improvement as well as the reduction of the costs in comparison with using only nano metal oxides for the remediation of environmental pollutants.

Triphenyltin chloride (TPT) is a biocide that has been used to prevent fouling organisms on ships, preserve wood, kill pests, and for other purposes (Ayanda et al. 2012b). Due to observed adverse effects on oysters, snails, and other aquatic animals, TPT has been considered a potential endocrine disrupting chemical (Golub and Doherty, 2004) and its use in ship paints has been banned by many nations. However, the use of TPT on ships and some uses other than as antifouling paints still continue due to the large economic benefits, hence a need to reduce the concentration of TPT in wastewater to > 99% before discharge into the environment. The physicochemical properties and structure of TPT are presented in Table 1.

Table 1. Physicochemical properties and structure of triphenyltin chloride

| | |
|--|---|
| Synonyms | Fentin Chloride; TPT; TPHT; TPTC |
| (CAS) Registry No | 639-58-7 |
| Molecular formula | C ₁₈ H ₁₅ ClSn |
| Structure |  |
| Molecular weight | 385.5 |
| Melting point | 106°C |
| Solubility in water (20°C) | 40 mg/L |
| Solubility in other solvents (20°C) | moderately soluble in organic solvent |
| Vapor pressure | 0.021 mPa |

In this study, CFAZ was prepared to enhance the physicochemical properties of CFA by modification with nZnO. The adsorption capacity of TPT in simulated seawater matrix onto the prepared CFAZ was then investigated.

Materials and methods

Reagents and adsorbent preparation

TPT (purity 98%), methanol, hexane, acetic acid, sodium hydroxide and sodium tetraethylborate (NaBEt₄) were purchased from Sigma Aldrich, USA while carbonate, sulphate

and chlorides salts for the preparation of simulated seawater were supplied by Merck. Stock solution containing 1000 mg/L TPT was prepared daily by dissolving TPT in methanol and stored in the dark at 4°C. Working solution of the derivatization agent (1% NaBEt₄) and acetate buffer (pH 4.5) were also prepared daily. TPT – contaminated simulated seawater was simulated in the laboratory by spiking simulated seawater with TPT stock solution. The simulated seawater was prepared by the method reported in Ayanda et al. 2013a while CFAZ (Fig. 1) involving CFA and nZnO in the ratio 1:1 was prepared by the method reported by Fatoki et al. 2012.

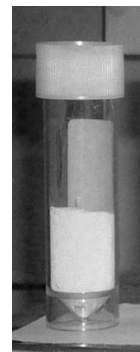


Fig. 1. Coal fly ash supported nZnO (CFAZ)

The physicochemical characterization of the precursors and CFAZ was carried out in order to understand the properties of the precursors that have been improved.

Instrumentation

The scanning electron micrographs (SEMs) of CFA, nZnO and CFAZ were viewed under a FEI™ scanning electron microscope (Nova Nano SEM 230). Euro Ea elemental analyzer was used to analyze the percentage of carbon content. Fourier transform infrared spectroscopy (FTIR) absorption spectra were obtained using the potassium bromide (KBr) pellet method and the spectra of the samples were recorded over the range 4 000–400 cm⁻¹ using Perkin Elmer™ Spectrum 1000. The specific surface area and porosity of these samples were obtained using a Tristar 3000 analyzer with N₂ adsorption at – 196°C. The pH, point of zero charge (PZC) by mass titration and ash content of the CFA, nZnO and CFAZ were also determined.

The equilibrium concentrations of TPT after adsorption were determined after derivatization by the use of gas chromatography – flame photometric detector (GC-FPD) (Shimadzu GC-2010 Plus) with a capillary column HP 5 (5% phenyl methyl siloxane, 30 m × 0.25 mm, i.d., film thickness 0.25 μm). The temperature was programmed as follows: initially at 60°C hold for 1 min, then heated to 280°C at 10°C/min, hold for 4 min. The injection and detector temperatures were 270°C and 300°C, respectively and the carrier gas was high purity helium. Gas chromatography – mass spectrometry (Agilent 6890N GC with CTC CombiPAL auto sampler and Agilent 5975B MS) analysis was also conducted to investigate if the adsorption of TPT onto CFAZ results in the degradation of TPT into other compounds or derivatives, and to check that the use of the adsorbent has not resulted in the production of a more severe pollutants during the treatment process. Table 2 shows the GC – MS instrument operating parameters.

Table 2. GC-MS operating parameters for the confirmation of TPT

| | |
|--------------------------------|--|
| GC injection parameters | |
| Mode | Splitless |
| Temperature | 270°C |
| Pressure | 98.6 kPa |
| Purge flow | 50.0 mL/min |
| Purge time | 10.00 min |
| Total flow | 54.3 mL/min |
| Gas saver | On |
| Saver flow | 50.0 mL/min |
| Saver time | 2.00 min |
| Gas type | Helium |
| Column parameters | |
| Column information | Rtx®-5MS , Restek 12723-127 |
| Max. temperature | 330°C |
| Normal Length | 30 m, 0.25 mm ID, 0.25 µm film thickness |
| Oven programme | initially at 60°C hold for 1 min, then heated to 280°C at 10°C/min, hold for 7 min |
| Mode | Constant flow |
| Initial flow | 1.6 mL/min |
| Normal initial pressure | 98.6 kPa |
| Average velocity | 46 cm/sec |
| Inlet | Front inlet |
| Outlet | MSD |
| Outlet pressure | Vacuum |

Adsorption experiments

The adsorption experiments of TPT onto CFAZ were conducted in a batch method, which permits complete evaluation of parameters that influence the adsorption process (Ayanda et al. 2013a). Adsorption experiments were conducted in which TPT – contaminated simulated seawater was introduced into 250 mL Erlenmeyer flasks containing accurately weighed amounts of CFAZ. The flasks were shaken by means of an orbital shaker at room temperature (20°C) for a prescribed length of time to obtain equilibrium. CFAZ was removed by filtration and the equilibrium concentrations of TPT determined. The concentration of TPT remaining in the solution was calculated by taking the difference of initial and final TPT concentrations. The adsorption capacities were obtained by mass balance equation (Equation 1):

$$q = \frac{(c_o - c_e)}{W} V \quad (1)$$

where q is the equilibrium adsorption capacity per gram dry weight of CFAZ, mg/g; c_o is the initial concentration of TPT in the solution, mg/L; c_e is the final or equilibrium concentration

of TPT in the solution, mg/L; V is the volume of the solution, L; and W is the dry weight of CFAZ, g.

Adsorption kinetics experiments were conducted at room temperature using 100 mg/L of TPT solutions with 0.5 g of CFAZ per 25 mL keeping pH at 8, a stirring speed of 200 rpm and a contact time of 10–70 min. The data obtained were analyzed with pseudo first-order, pseudo second-order, Elovich, fractional power and intraparticle diffusivity kinetic models.

The effect of pH on TPT adsorption was studied by varying the pH in the range of 3 to 9, the effect of stirring speed on TPT adsorption was studied by varying the mixing speeds from 160 to 200 rpm and the effect of temperature was evaluated after the optimization of all the working parameters for TPT adsorption at initial TPT concentration of 100 mg/L solution with 0.5 g of adsorbents per 25 mL, pH 8, contact time of 60 min and stirring speed of 200 rpm from where the thermodynamic parameters of TPT adsorption in simulated seawater were obtained.

The adsorption isotherms were investigated by varying the initial TPT concentration from 12.5 to 200 mg/L at optimized adsorbent dose, contact time, pH and stirring speed established after optimization of working parameters. The equilibrium data were fitted by Langmuir, Freundlich, Temkin and D-R isotherm models.

Results and discussion

Characterization of the precursors and CFAZ

The SEM of CFA (Fig. 2a) showed that each of the particles of CFA is spherical with smooth and regular surfaces. The size of the spheres was found to be 0.6–26.2 μm with a mean particle size of $3.2 \pm 3.9 \mu\text{m}$. The SEM of nZnO (Fig. 2b) showed that the nZnO particles consist of uniform granules with more regular surfaces. The SEM presents granules of particle sizes ranging from between 15.9–144.7 nm with a mean particle size of $53.5 \pm 26.6 \text{ nm}$. The SEM of CFAZ (Fig. 2c) thus showed that the CFA and nZnO particles were clustered together with large intergranular voids and crevices found. The SEM also showed that the CFA and nZnO particles maintained their morphology after the preparation of CFAZ.

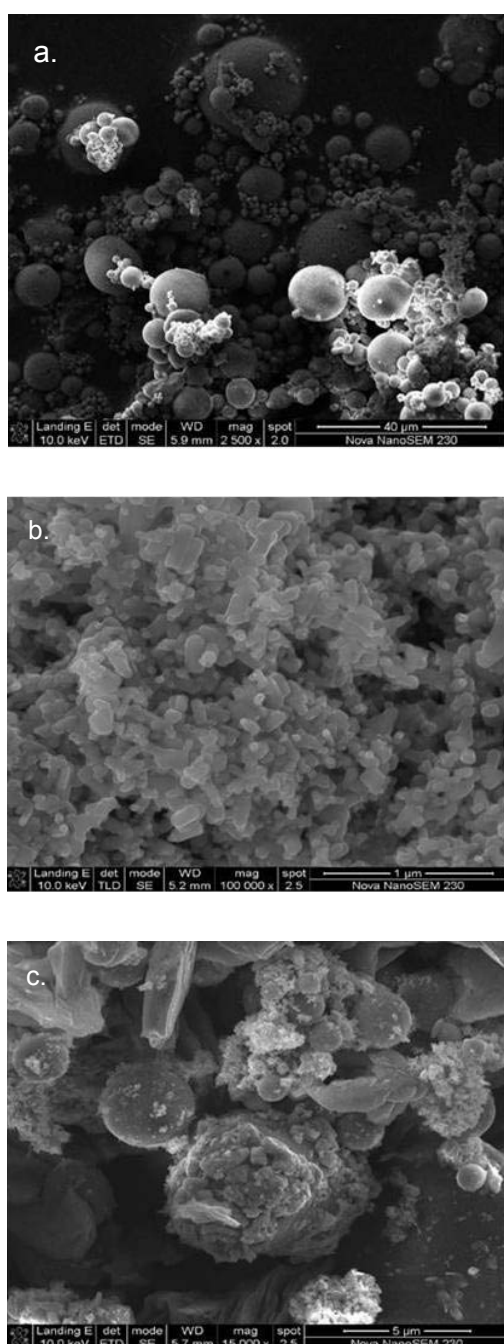
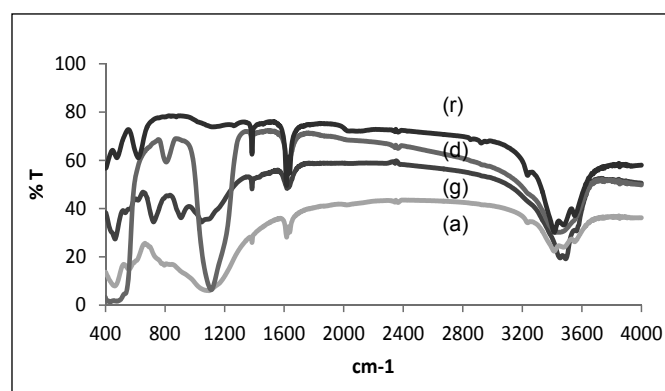


Fig. 2. SEM of CFA (a), nZnO (b) and CFAZ (c)

In the FTIR spectrum of CFAZ (Fig. 3), the absorption at 1097 cm^{-1} (curve (a)) is assigned to the C–C stretching of CFA while the absorption at 1110 cm^{-1} (curve (d)) is assigned to the Zn–O stretching of nZnO and the absorption at 808 cm^{-1} (curve (d)) is assigned to the Zn–O stretching of nZnO. It was found that the wavenumber of Zn–O stretching shifted from 808 cm^{-1} of nZnO to 722 cm^{-1} (curve (g)) of CFAZ. The wavenumber of the absorption peak decreased by 86 cm^{-1} .



(r) – Reference (KBr), (d) – nZnO, (g) – CFAZ, (a) – CFA

Fig. 3. FTIR spectrum of CFA, nZnO and CFAZ

The decreased wavenumber for the absorption peak indicated that the strength of Zn–O bond decreased. It could also be explained that a new C–O–Zn bond was formed during the preparation of the CFAZ.

Results obtained on the BET surface area and porosity determination of the precursors and CFAZ showed that the surface areas of nZnO and CFA are 14.41 ± 0.039 and $1.06 \pm 0.003 \text{ m}^2/\text{g}$, respectively while the surface area of CFAZ is $198.45 \pm 0.09 \text{ m}^2/\text{g}$. The surface areas of nZnO and CFA were therefore increased by 92.74 and 99.47%, respectively. The micropore area of CFAZ was $5.44 \text{ m}^2/\text{g}$ while the micropore areas of CFA, and nZnO were 0.380 and $3.18 \text{ m}^2/\text{g}$, respectively. These values were thus smaller than the micropore area of the CFAZ. The results showed that the use of CFA and nZnO for the preparation of CFAZ greatly accelerated the surface and micropore area of CFA. The increase in the surface and micropore areas might be as a result of the formation of large vacant sites (intergranular voids and crevices) after the preparation of CFAZ, this is supported by the SEM images. Other properties of CFA, nZnO and CFAZ are presented in Table 3.

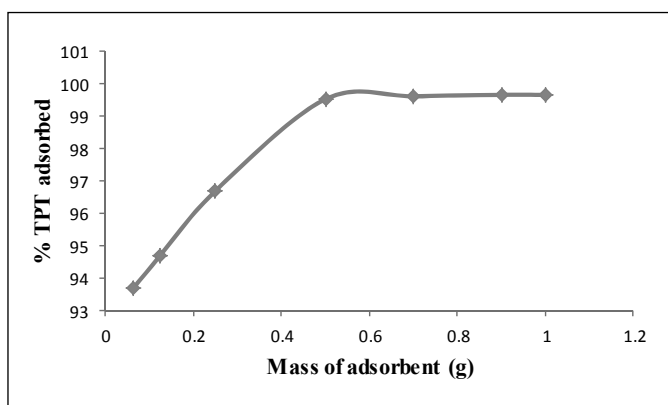
CFAZ was chosen for the adsorption of TPT based on improved surface morphology (large intergranular voids and crevices), higher surface area and porosity when compared with CFA and nZnO.

Effect of adsorbent amount

To study the effect of adsorbent amount on the adsorption of TPT from TPT – contaminated simulated seawater, the amount of CFAZ was varied from 0.0625–1.0 g, the concentration of TPT was taken as 100 mg/L and other parameters were also kept constant. Fig. 4 shows that the amount of TPT adsorbed and the percentage removal of TPT by the CFAZ increases as the amount of nZnO increases from 0.0625–0.5 g after which equilibration was attained.

Table 3. Physicochemical properties of CFA, nZnO and CFAZ

| Characteristics | CFA | nZnO | CFAZ |
|--|------------------------|------------------|-------------------|
| pH | 10.70 | 6.71 | 6.96 |
| PZC | 12.17 | 6.71 | 6.70 |
| Particle size | 0.6–26.2 μm | 15.9–144.7 nm | – |
| Surface area (m^2/g) | 1.06 ± 0.003 | 14.41 ± 0.04 | 198.45 ± 0.09 |
| Micropore area (m^2/g) | 0.38 | 3.18 | 5.44 |
| Ash content (%) | 97.40 ± 0.14 | 99.20 ± 0.14 | 85.90 ± 0.01 |
| Carbon content (%) | 1.54 | 0.42 | 0.79 |

**Fig. 4.** Adsorption efficiencies of TPT onto CFAZ

Experimental conditions: Concentration of TPT = 100 mg/L;
Volume of TPT solution = 25 mL,
Contact time = 60 min; Stirring speed = 160 rpm, Temperature = 20°C.

The figure therefore shows that 0.5 g CFAZ removes 99.63% of TPT from 25 mL of TPT – contaminated simulated seawater at a contact time of 60 min, stirring speed of 160 rpm and temperature of 20°C. 0.5 g was chosen and used for further studies.

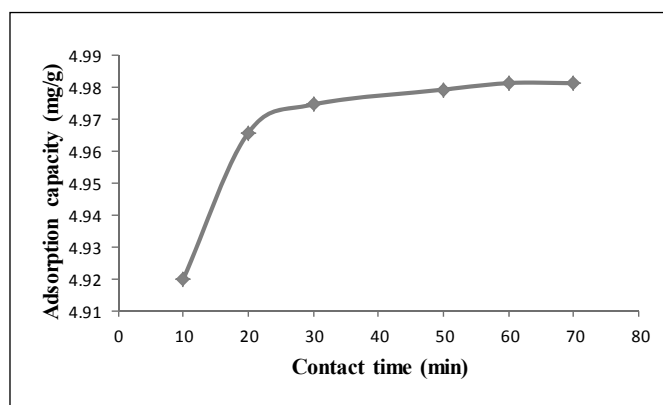
Effect of contact time

For the effect of contact time on the adsorption of TPT onto CFAZ, the TPT concentration was 100 mg/L while, other remaining conditions such as pH, stirring speed etc. were constant. The effect of contact time was carried out at various time intervals from 10–70 min. The increase in the amount of TPT adsorbed by CFAZ from 4.9198 mg/g (98.40%) to 4.9814 mg/g (99.63%) (Fig. 5) was observed up to 60 min. After that, there is no significant change observed.

This can be attributed to the fact that a large number of vacant surface sites are available for adsorption at the initial stage, and after a lapse of time (60 min), the remaining vacant surface sites were difficult to be occupied due to repulsive forces between the solute molecules on the solid and bulk phases (Bazrafshan et al. 2012). A contact time of 60 min was therefore fixed as the time used for further studies.

Adsorption kinetics

Pseudo first-order, pseudo second-order, Elovich, fractional power and intraparticle diffusion rate equations have been

**Fig. 5.** Effect of contact time on TPT adsorption onto CFAZ

Experimental conditions: Concentration of TPT = 100 mg/L;
Volume of TPT solution = 25 mL,
Mass of CFAZ = 0.5 g; Stirring speed = 160 rpm, Temperature = 20°C.

used for modeling the kinetic of TPT adsorption onto CFAZ as presented in Equation 2–6, respectively.

The pseudo first-order kinetics is linearly expressed as:

$$\log(q_e - q_t) = \log q_e - \frac{k_1}{2.303}(t) \quad (2)$$

where, q_e is the amount of TPT adsorbed at equilibrium per unit weight of the CFAZ (mg/g); q_t is the amount of TPT adsorbed at any time (mg/g) and k_1 is the pseudo first – order rate constant/min. The values of $\log(q_e - q_t)$ were linearly correlated with t . The plot of $\log(q_e - q_t)$ versus t should give a linear relationship from which k_1 and q_e can be determined from the slope and intercept of the plot, respectively.

The pseudo second-order rate expression is given by:

$$\frac{t}{q} = \frac{1}{k_2 q_e^2} + \frac{1}{q_e}(t) \quad (3)$$

where, k_2 is the rate constant of pseudo second – order adsorption ($\text{g}/\text{mg min}$). If the second-order kinetics is applicable, the plot $\frac{t}{q}$ against t in Equation 3 should give a linear relationship from where the constants q_e and k_2 can be determined. Moreover, the

initial adsorption rate h (mg/g/min) can be determined using the equation $h = k_2 q_e^2$ (Basha and Murthy, 2007).

The Elovich equation is expressed as:

$$q_t = \frac{1}{\beta} \cdot \ln \frac{\alpha_E}{\beta} + \frac{1}{\beta} \cdot \ln t \quad (4)$$

where, α_E and β are the constants during any one experiment (α_E is the initial TPT sorption rate and β is the desorption constant). A plot of q_t vs $\ln t$ should give a linear relationship with a slope of $\frac{1}{\beta}$ and an intercept of $\frac{1}{\beta} \cdot \ln \frac{\alpha_E}{\beta}$ (Aboul-Kassim and Simoneit, 2001).

The linear form of the fractional power model is expressed as:

$$\log q_t = \log k_3 + v \log t \quad (5)$$

where, k_3 is a constant, t is time, and v is a positive constant (< 1). A plot of $\log q_t$ vs $\log t$ should give a linear relationship with a slope (v) and an intercept of $\log k_3$.

The intraparticle diffusion rate equation is expressed as:

$$q_t = I + k_p t^{0.5} \quad (6)$$

where, k_p is the intraparticle diffusivity constants, t is time, and I is the boundary layer diffusion effects. q_t was plotted against

time $t^{0.5}$ and the rate coefficient k_p and boundary layer diffusion effects I calculated from the slope and intercept of the graph, respectively (Boparai et al. 2010).

Fig. 6 thus shows the pseudo first-order, pseudo second-order, Elovich, and fractional power kinetic plots. Fig. 7 presents the intraparticle diffusivity kinetic plot and Table 4 shows the evaluated parameters of all the kinetics models.

The value of the correlation coefficient (R^2) of pseudo second-order kinetic model (> 0.99) is higher than the correlation coefficients of other models indicating that the kinetic model for the adsorption of TPT onto CFAZ is pseudo second-order (Ayanda et al. 2013b). The value of the initial adsorption rate, h , obtained for the pseudo second-order kinetics is 42.918 mg/g/min. This reveals that the initial adsorption rate (' h ' value) was high and a somewhat complex mechanism of adsorption instead of single step process. The amount of TPT adsorbed at equilibrium per unit weight of CFAZ (q_e) is 4.990 mg/g and the rate constant of pseudo second-order adsorption (k_2) is 1.7236 g/mg/min. The results also indicate that the power function model satisfactorily describes the time-dependence of TPT on the CFAZ since the value of the constant v is less than 1.

Adsorption mechanisms

According to Boparai et al. 2010, the overall rate of adsorption can be described by: (1) surface diffusion where the adsorbate is transported from the bulk solution to the external surface of adsorbent, (2) intraparticle diffusion where the adsorbate molecules move into the interior of sorbent particles, and (3) adsorption on the interior sites of the adsorbent. Since the

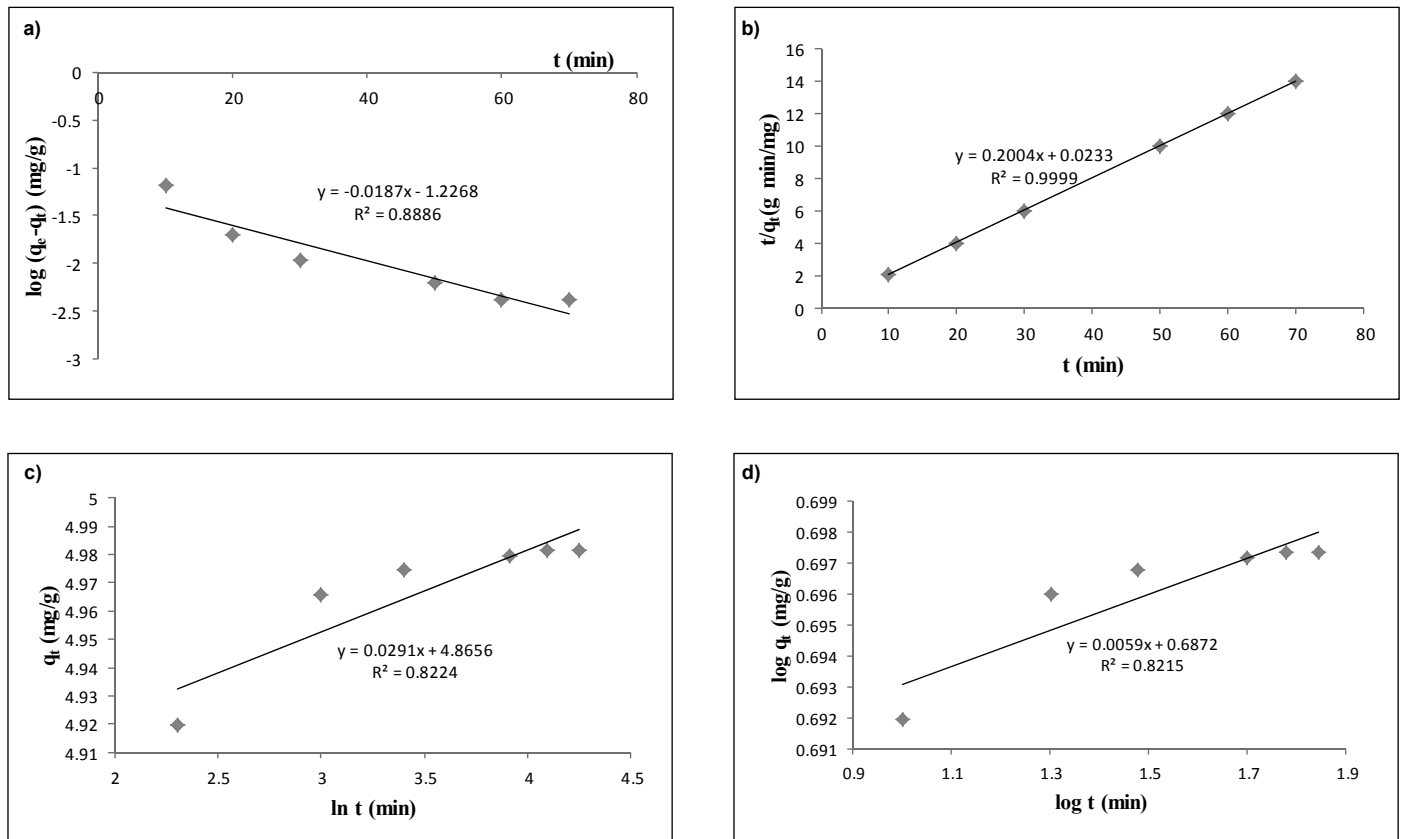
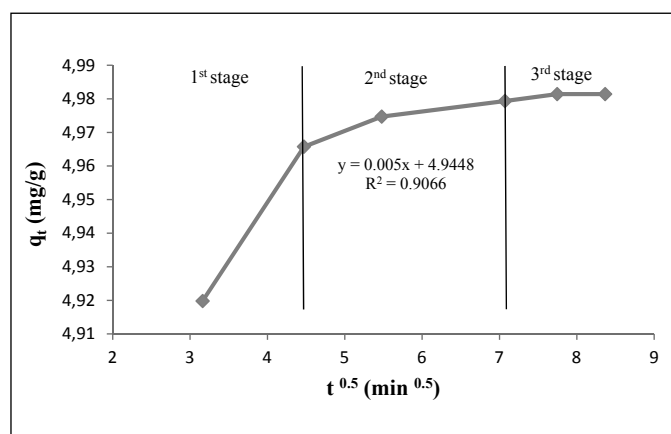


Fig. 6. Pseudo first-order (a), Pseudo second-order (b), Elovich (c), and fractional power (d) rate equation plot for TPT adsorption onto CFAZ

Table 4. Kinetic model parameters for TPT adsorption onto CFAZ

| Kinetic models | Parameters |
|-----------------------------------|------------------------|
| Pseudo first-order | |
| k_1 (min ⁻¹) | 0.04307 |
| q_e (mg/g) | 0.05932 |
| R^2 | 0.8886 |
| Pseudo second-order | |
| q_e (mg/g) | 4.990 |
| h (mg/g/min) | 42.918 |
| k_2 (g/mg/min) | 1.7236 |
| R^2 | 0.9999 |
| Elovich | |
| β (g min/mg) | 34.3643 |
| α (g min ² /mg) | 1.417×10^{74} |
| R^2 | 0.8224 |
| Fractional Power | |
| v (min ⁻¹) | 0.0059 |
| k_3 (mg/g) | 4.8663 |
| k_3v (mg/g/min) | 0.0287 |
| R^2 | 0.8215 |
| Intraparticle diffusivity | |
| k_p (min ⁻¹) | 0.005 |
| I | 4.9448 |
| R^2 | 0.9066 |

adsorption step is very rapid, it is assumed that it does not influence the overall kinetics. The overall rate of adsorption process, therefore, will be controlled by either surface diffusion or intraparticle diffusion. Equation 6 was used to determine if intraparticle diffusion is the rate-limiting step for the adsorption of TPT onto CFAZ.

**Fig. 7.** Intraparticle diffusivity plot for TPT adsorption onto CFAZ

The intraparticle kinetic plots may present a multilinearity (Annadurai et al. 2002), indicating that two or more steps take place. The first, sharper portion is the instantaneous adsorption stage, the second portion is the gradual adsorption stage, where intraparticle diffusion is rate-controlled and the third portion is the final equilibrium stage where intraparticle diffusion starts to slow down due to extremely low adsorbate concentrations in the solution. As shown in Fig. 7, the instantaneous adsorption stage (stage 1) is completed before 20 min, and then the stage of intraparticle diffusion control (stage 2) is attained and continues from 20 to 40 min. Finally, the final equilibrium adsorption (stage 3) starts after 40 min. This showed that TPT is slowly transported via intraparticle diffusion into the particles and is finally retained in the micropores. In general, the slope of the line in stage 2 is referred to as the intraparticle diffusion rate constant, k_p .

Effect of pH

The effect of pH on the adsorption of TPT onto CFAZ was studied at pH 4–9. It was observed from Fig. 8 that the percentage of TPT adsorbed by the CFAZ steadily increases as the pH of the solution increases from pH 4 to pH 8, and reaches equilibration afterwards.

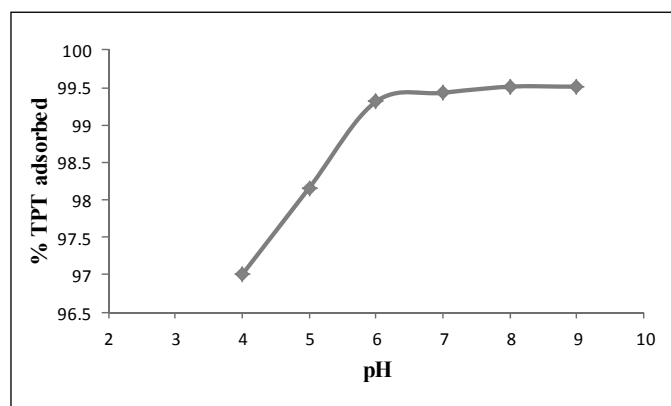


Fig. 8. Effect of pH on TPT adsorption onto CFAZ

Experimental conditions: Concentration of TPT = 100 mg/L; Volume of TPT solution = 25 mL, Mass of CFAZ = 0.5 g; Contact time = 60 min; Stirring speed = 160 rpm, Temperature = 20°C.

Approx. 99.51% of TPT was removed from the initial concentration of 100 mg/L TPT by the CFAZ at a contact time of 60 min, stirring speed of 160 rpm, temperature of 20°C and pH 8. pH 8 was chosen as the optimum pH and was used for further studies.

Effect of stirring speed

The stirring speed on the adsorption of TPT onto CFAZ was studied at a stirring speed of 160–200 rpm. Fig. 9 shows that the adsorption capacity of TPT onto the CFAZ increases as the stirring speed of the mixture increases from 160 to 190 rpm, and reaches equilibration at 190–200 rpm.

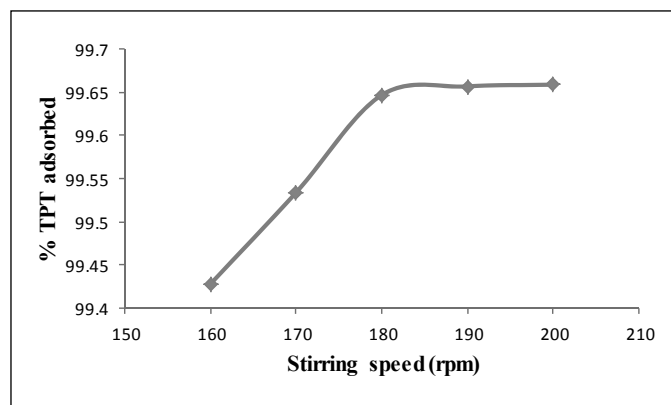


Fig. 9. Effect of stirring speed on TPT adsorption onto CFAZ

Experimental conditions: Concentration of TPT = 100 mg/L; Volume of TPT solution = 25 mL, Mass of CFAZ = 0.5 g; Contact time = 60 min; Temperature = 20°C.

The figure therefore shows that 99.66% of TPT was removed from the initial concentration of 100 mg/L TPT by the CFAZ at a contact time of 60 min, pH 8, temperature of 20°C and a stirring speed of 200 rpm. A stirring speed of 200 rpm was used for further studies.

Adsorption isotherms

The adsorption equilibrium data were analyzed by Langmuir, Freundlich, Temkin and D-R adsorption models (Equation 7–10).

$$\frac{c_e}{c_a} = \frac{1}{A_{\max} k_L} + \frac{1}{A_{\max}} c_e \quad (7)$$

where, c_e (mg/L) is the equilibrium concentration of TPT in the solution, c_a (mg/g) is the TPT adsorption capacity for the CFAZ at equilibrium, A_{\max} (mg/g) is the maximum monolayer TPT adsorption capacity, and k_L (L/mg) is the Langmuir isotherm constant related to the free energy of adsorption. The values of A_{\max} and k_L were calculated from the intercept and the slope of the straight line of the linearized form of the Langmuir isotherm.

$$\log c_a = \log k_F + \frac{1}{n_F} \log c_e \quad (8)$$

where, k_F [$\text{mg/g} (\text{L/mg})^{1/n}$] and n_F are the Freundlich constants which are related to the adsorption capacity and adsorption intensity, respectively. The values of k_F and n_F were obtained from the intercept and the slope of the straight line of the linearized form of the Freundlich isotherm, respectively.

$$c_a = n_T \ln k_T + n_T \ln c_e \quad (9)$$

where, $n_T = \frac{RT}{b_T} \log c_e$, b_T is the Temkin constant related to the heat of sorption (J/mol) and k_T is the Temkin isotherm constant (L/g). The values of n_T , b_T and k_T were obtained from the intercept and the slope of the straight line of the linearized form of the Temkin isotherm.

$$\ln c_a = \ln q_m - k_{D-R} \varepsilon^2 \quad (10)$$

where q_m is the maximum TPT adsorption capacity (mg/g), k_{D-R} is the D–R constant related to free energy, R (8.314 J/mol K) is the gas constant, T (K) is the absolute temperature and ε

is the Polanyi potential which is defined as $\varepsilon_T = RT \ln \left(1 + \frac{1}{c_e} \right)$.

The values of q_m and k_{D-R} were calculated from the intercept and the slope of the straight line of the linearized form of the D-R isotherm while the mean free energy (E) was calculated

$$\text{using } E = \frac{1}{\sqrt{2k_{D-R}}}.$$

The graphs of the adsorption isotherms are presented in Fig. 10 and the parameters obtained for the models were given in Table 5. The Table 5 and Fig. 10 show that the experimental data fitted well with the Freundlich isotherm model (i.e regression coefficient ($R^2 > 0.99$) is higher than that for other models), probably due to the real heterogeneous nature of the surface sites involved in the process of adsorption (Han et al. 2007). The surface morphology of CFAZ (Fig. 2c) also confirms that the surface of the adsorbent is non-uniform. The value of n_F , falling in the range 1–10 also indicates favorable adsorption.

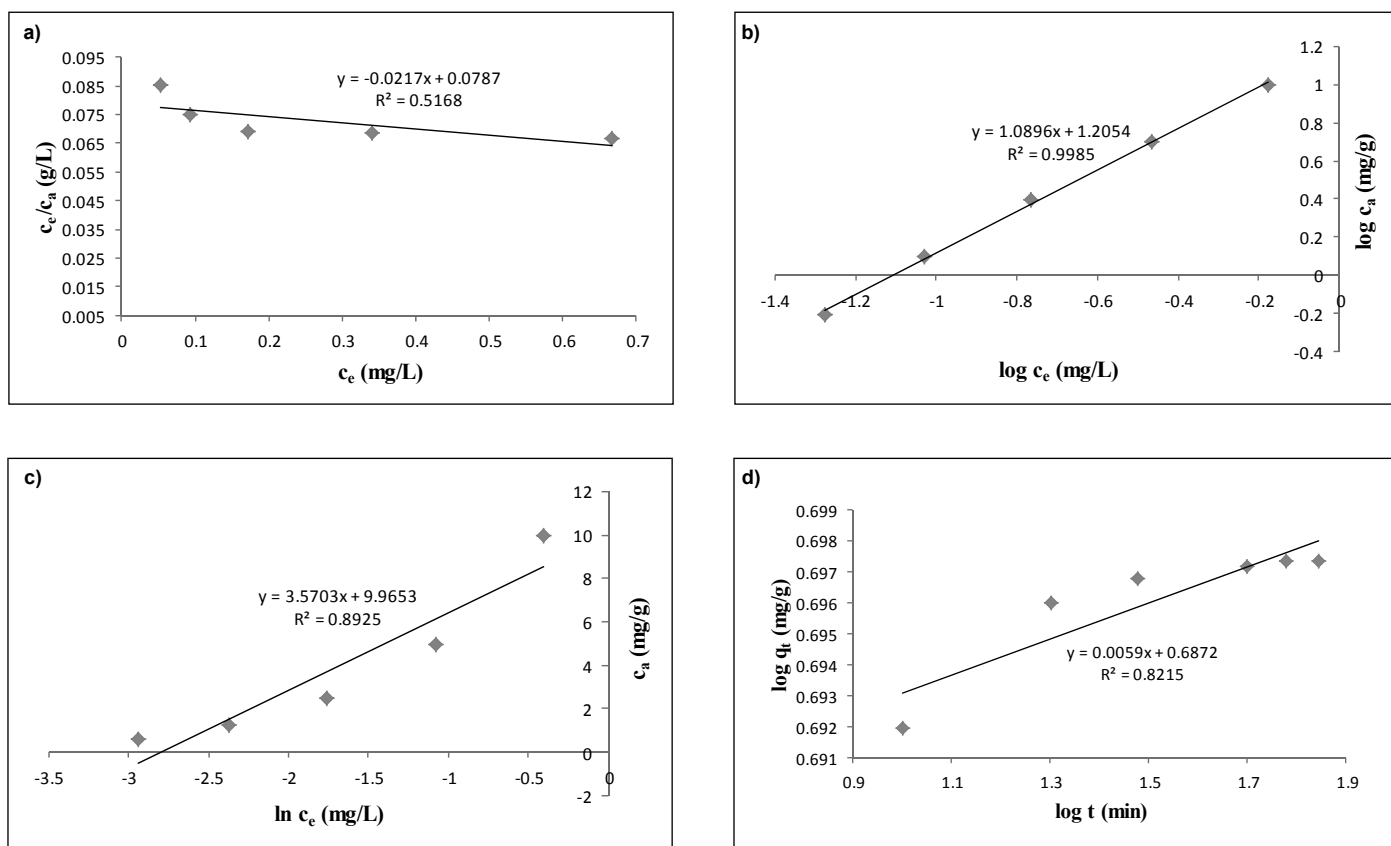


Fig. 10. Langmuir (a), Freundlich (b), Temkin (c), and D-R (d) isotherms for adsorption of TPT onto CFAZ

Table 5. Isotherms constants for the adsorption of TPT onto CFAZ

| Equilibrium models | Parameters |
|---|----------------------|
| Freundlich | |
| K_F [mg/g (L/mg) ^{1/n}] | 16.047 |
| n_F | 0.9178 |
| R^2 | 0.9985 |
| Langmuir | |
| K_L (L/mg) | -0.2757 |
| A_{max} (mg/g) | -46.083 |
| R^2 | 0.5168 |
| Temkin | |
| n_T (L/g) | 3.5703 |
| k_T (mg/L) | 16.300 |
| b_T (J/mol) | 682.296 |
| R^2 | 0.8925 |
| D-R | |
| k_{D-R} (J ² /mol ²) | 4.0×10^{-8} |
| q_m (mg/g) | 10.2185 |
| E (J/mol) | 3535.53 |
| R^2 | 0.9694 |

The negative value of the Langmuir constants, A_{\max} (mg/g) and k_L (L/mg) for TPT adsorption onto CFAZ (Table 5) indicates the inadequacy fitting of experimental data to Langmuir model. The equilibrium model constants k_F , k_L , k_T and k_{D-R} for the adsorption of TPT onto CFAZ material are 16.047 mg/g (L/mg)^{1/n}, -0.2757 L/mg, 16.30 mg/L and 4.0×10^{-8} J²/mol², respectively.

Effect of temperature

The experimental results obtained on the effect of temperature show that the adsorption capacity of TPT onto CFAZ decreases with increase in the solution temperature (Fig. 11a). This indicates that the adsorption of TPT onto the CFAZ is exothermic (Han et al. 2007, Ayanda et al. 2013b). The thermodynamic parameters were determined from the thermodynamic equilibrium constant, K_c . The standard Gibbs free energy ΔG° (kJ/mol) was calculated using Equation 11 while the values of the standard enthalpy change ΔH° (kJ/mol) and standard entropy change ΔS° (J/K/mol) can be calculated from the intercept and the slope of the linear plot of $\log K_c$ versus $\frac{1}{T}$ (Equation 12b). K_c was calculated by the use of Equation 12a.

$$\Delta G^\circ = -RT \ln K_c \quad (11)$$

$$K_c = \frac{c_a}{c_e} \quad (12a)$$

$$\log K_c = \frac{\Delta S^\circ}{2.303R} - \frac{\Delta H^\circ}{2.303R} \cdot \frac{1}{T} \quad (12b)$$

where, c_a (mg/L) is the amount of the TPT (mg) adsorbed on the adsorbent per liter of the solution at equilibrium, c_e (mg/L) is the equilibrium concentration of TPT in the solution, R is the universal gas constant, 8.314 J/mol K; T is absolute temperature and K_c is the thermodynamic equilibrium constant.

From Fig. 11a, approx. 99.07% of TPT was removed from the initial concentration of 100 mg/L TPT by CFAZ at a contact time of 60 min, pH 8, stirring speed 200 rpm and temperature of 80°C, whereas 99.55% TPT was removed at 40°C at the same conditions. Fig. 11b thus shows the Van't Hoff plot for the adsorption of TPT and the variation in the extent of adsorption with respect to temperature (ΔH° , ΔS° and ΔG°) are presented in Table 6.

The negative value of ΔH° (-16.159 kJ/mol) for the intervals of temperatures studied (Table 6) also shows the exothermic nature of the adsorption process. The negative value of ΔS° (-6.5368 J/K/mol) corresponds to a decrease in the degree of freedom of the adsorbed TPT, indicating a decrease in TPT concentration onto the solid phase. ΔG° values were found to increase as the temperature increases, this indicated that the adsorption efficiency of TPT onto CFAZ decreases with increase in temperature.

Application of laboratory findings to real matrix

Optimal conditions obtained (through laboratory findings) for the adsorption of TPT from contaminated simulated seawater were applied to TPT removal from real matrix (TPT – contaminated natural seawater obtained from the Cape Town harbor). Approx. 99.60% TPT was removed by 0.5 g of CFAZ after adsorption of TPT contained in 25 mL of contaminated natural seawater at a contact time of 60 min, stirring speed of 200 rpm and at pH 8.

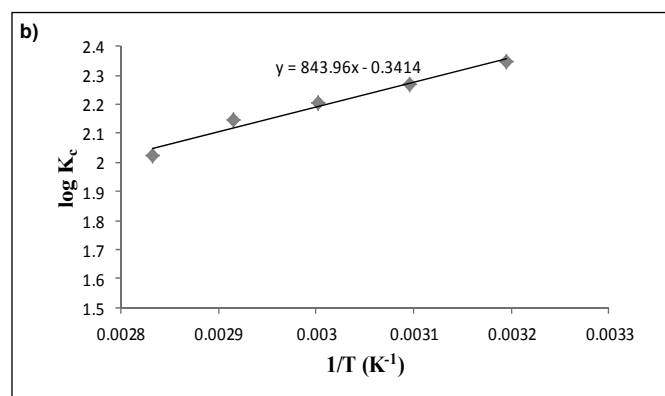
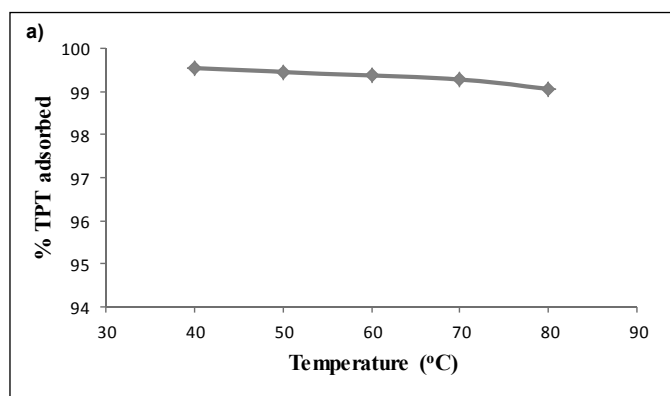


Fig. 11. Effect of temperature (a) and Van't Hoff Plot (b) for TPT adsorption onto CFAZ

Experimental conditions: Concentration of TPT = 100 mg/L; Volume of TPT solution = 25 mL, Mass of CFAZ = 0.5 g; Contact time = 60 min; pH = 8; Stirring speed = 200 rpm.

Table 6. Thermodynamic parameters for adsorption of TPT onto CFAZ

| Temperature (°C) | ΔG° (kJ/mol) | ΔS° (J/K/mol) | ΔH° (kJ/mol) | K_c |
|------------------|---------------------------|----------------------------|---------------------------|--------|
| 40 | -14.062 | -6.5368 | -16.159 | 222.21 |
| 50 | -14.027 | | | 185.57 |
| 60 | -14.042 | | | 159.51 |
| 70 | -14.080 | | | 139.43 |
| 80 | -13.688 | | | 106.07 |

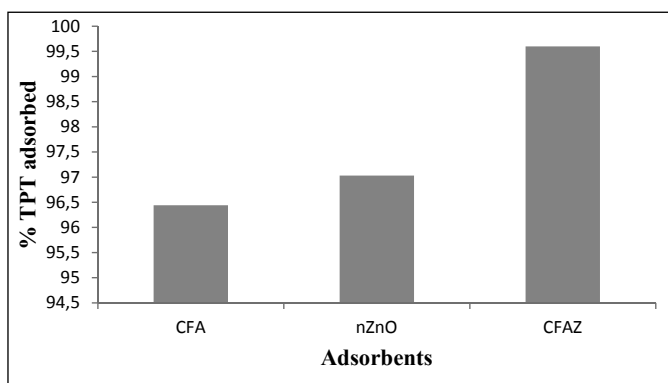


Fig. 12. Percentage TPT removed from contaminated natural seawater

These conditions were also applied to the CFA and nZnO and the results (Fig. 12) showed that approx. 96.44% and 97.03% TPT were removed from the contaminated natural seawater by the CFA and nZnO, respectively. The order of increasing TPT adsorption capacity was thus: CFA < nZnO < CFAZ.

3.11 TPT confirmation after adsorption by GC-MS

Fig. 13a shows the GC-MS spectra of TPT remaining in solution after adsorption of 100 mg/L TPT with 0.5 g of CFAZ at a contact time of 60 min, temperature 20°C, pH 8 and

a stirring speed of 200 rpm. The GC-MS library match spectra is presented in Fig. 13b.

The MS fragmentation patterns of TPT therefore match very well with TPT spectra library which confirmed that the TPT was not degraded into other toxic compounds or other forms of derivatives during the process of adsorption.

Conclusions

From the present study, it can be seen that the CFAZ can be used effectively for the removal of TPT from contaminated seawater. The percentage removed was found to depend on all the operating factors, *viz.* adsorbent dose, contact time, solution pH, stirring speed, initial concentration and temperature. The equilibrium data can well be described by the Freundlich isotherm and the kinetic data followed the pseudo second-order kinetic model. The thermodynamic analysis also showed that the adsorption process was exothermic. CFAZ was able to remove up to 99.60% TPT contained in 25 mL of contaminated natural seawater at a contact time of 60 min, stirring speed of 200 rpm and at pH 8. GC-MS analysis also confirmed that TPT was not degraded into other forms of compounds/derivatives or toxic substance during the process of adsorption. CFAZ can therefore be effectively used for the treatment of shipyard process wastewater before discharge into the marine environment.

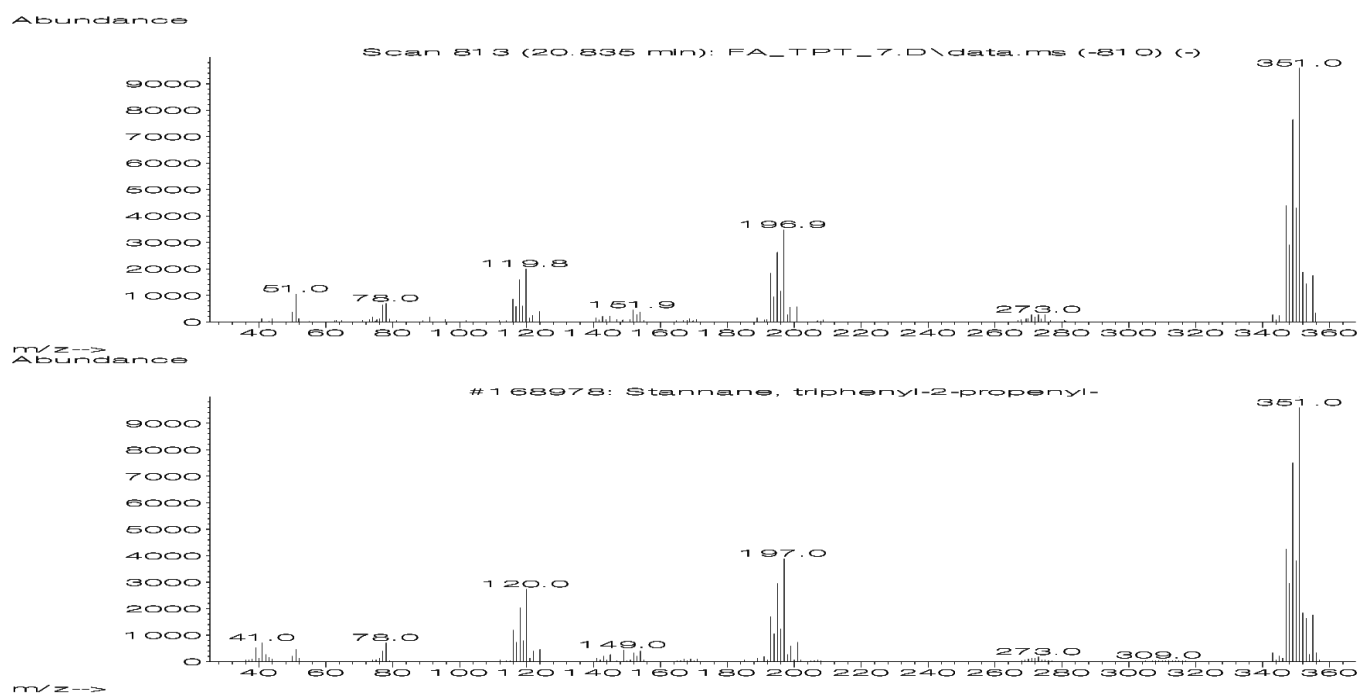


Fig. 13. GC-MS spectra of TPT (a) and the library match spectra (b)

References

- [1] Aboul-Kassim, T.A.T. & Simoneit, B.R.T. (2001). *Sorption/desorption of organic pollutants from complex mixtures: Modeling, kinetics, experimental techniques and transport parameters*, The Handbook of Environmental Chemistry, 5, Part E, pp. 1–74 Springer-Verlag, Berlin 2001.
- [2] Ada, K., Ergene, A., Tan, S. & Yalcin, E. (2009). Adsorption of remazol brilliant blue R using ZnO fine powder: equilibrium, kinetic and thermodynamic modeling studies, *Journal of Hazardous Materials*, 165, pp. 637–644.

- [3] Annadurai, G., Juang, R.S. & Lee, D.J. (2002). Use of cellulose based wastes for adsorption of dyes from aqueous solutions, *Journal of Hazardous Materials*, 92, pp. 263–274.
- [4] Ayanda, O.S., Fatoki, O.S., Adekola, F.A. & Ximba, B.J. (2012a). Characterization of fly ash generated from Matla power station in Mpumalanga, South Africa, *E-Journal of Chemistry*, 9, pp. 1788–1795.
- [5] Ayanda, O.S., Fatoki, O.S., Adekola, F.A. & Ximba, B.J. (2012b). Fate and remediation of organotin compounds in seawaters and soils, *Chemical Science Transactions*, 1, pp. 470–481.
- [6] Ayanda, O.S., Fatoki, O.S., Adekola, F.A. & Ximba, B.J. (2013a). Removal of tributyltin from shipyard process wastewater by fly ash, activated carbon and fly ash/activated carbon composite: Adsorption models and kinetics, *Journal of Chemical Technology and Biotechnology*, 88, pp. 2201–2208.
- [7] Ayanda, O.S., Fatoki, O.S., Adekola, F.A. & Ximba, B.J. (2013b). Utilization of nSiO₂, fly ash and nSiO₂/fly ash composite for the remediation of triphenyltin (TPT) from contaminated seawater, *Environmental Science and Pollution Research*, 20, pp. 8172–8181.
- [8] Basha, S. & Murthy, Z.V.P. (2007). Kinetics and equilibrium models for biosorption of Cr(VI) on chemically modified seaweeds, *Cystoseira indica*, *Process Biochemistry*, 42, pp. 1521–1529.
- [9] Bazrafshan, E., Mostafapour, F.K. & Zazouli, M.A. (2012). Methylene blue (cationic dye) adsorption into *Salvadora persica* stems ash, *African Journal of Biotechnology*, 11, pp. 16661–16668.
- [10] Boparai, H.K., Joseph, M. & O'Carroll, D.M. (2010). Kinetics and thermodynamics of cadmium ion removal by adsorption onto nano zerovalent iron particles, *Journal of Hazardous Material*, 186, pp. 458–465.
- [11] Golub, M. & Doherty, J. (2004). Triphenyltin as a potential human endocrine disruptor, *Journal of Toxicology and Environmental Health Part B*, 281–295.
- [12] Dunens, O.M., Mackenzie, K.J. & Harris, A.T. (2009). Synthesis of multiwalled carbon nanotubes on fly ash derived catalysts, *Environmental Science and Technology*, 43, pp. 7889–7894.
- [13] Fatoki, O.S., Ayanda, O.S., Adekola, F.A., Ximba, B.J. & Opeolu, B.O. (2012). Preparation and characterization of activated carbon – nFe₃O₄, activated carbon – nSiO₂ and activated carbon – nZnO hybrid materials, *Particle and Particle Systems Characterization*, 29, pp. 178–191.
- [14] Han, Z., Du, T. & Zhao, Y. (2007). Adsorption of triphenyltin chloride on modified chitosan, *Journal of Agro-Environment Science*, 5, pp. 1992–1995.
- [15] Juan, R., Hernandez, S., Querol, X., Andres, J.M. & Moreno, N. (2002). Zeolite material synthesized from fly ash: Use as cationic exchanger, *Journal of Chemical Technology and Biotechnology*, 77, pp. 299–304.
- [16] Nascimento, N., Soares, P.S.M. & Souza, V.P. (2009). Adsorption of heavy metal cations using coal fly ash modified by hydrothermal method, *Fuel*, 88, pp. 1714–1719.
- [17] Nath, D.C.D., Bandyopadhyay, S., Boughton, P., Yu, A., Blackburn, D. & White, C. (2010a). High strength biodegradable poly(vinyl alcohol)/fly ash composite films, *Journal of Applied Polymer Science*, 117, pp. 114–121.
- [18] Nath, D.C.D., Bandyopadhyay, S., Campbell, J., Yu, A., Blackburn, D. & White, C. (2010b). Surface-coated fly ash reinforced biodegradable poly(vinyl alcohol) composite films: Part 2-analysis and characterization, *Applied Surface Science*, 257, pp. 1216–1221.
- [19] Papandreou, A., Stournaras, C.J. & Panyas, D. (2007). Copper and cadmium adsorption on pellets made from fired coal fly ash, *Journal of Hazardous Materials*, 148, pp. 538–547.
- [20] Penilla, P.R., Bustos, A.G. & Elizalde, S.G. (2006). Immobilization of Cs, Cd, Pb and Cr by synthetic zeolites from Spanish low-calcium coal fly ash, *Fuel*, 85, pp. 823–832.
- [21] Poursaberi, T., Kono, E., Sarrafi, A.H.M., Hassanisadi, M. & Hajifathli, F. (2012). Application of nanoscale zero-valent iron in the remediation of DDT from contaminated water, *Chemical Science Transactions*, 1, pp. 658–668.
- [22] Querol, X., Moreno, N., Umana, J.C., Alastuey, A., Hernandez, E., Lopez-Soler, A. & Plana, F. (2002). Synthesis of zeolites from coal fly ash: an overview, *International Journal of Coal Geology*, 50, pp. 413–423.
- [23] Rohatgi, P.K., Gupta, N. & Alaraj, S. (2006). Thermal expansion of aluminum–fly ash cenosphere composites synthesized by pressure infiltration technique, *Journal of Composite Materials*, 40, pp. 1163–1173.
- [24] Salehi, R., Arami, M., Mahmoodi, N.M., Bahrami, H. & Khorramfar, S. (2010). Novel biocompatible composite (chitosan–zinc oxide nanoparticle): preparation, characterization and dye adsorption properties, *Colloids and Surfaces B*, 80, pp. 86–93.
- [25] Wang, S. (2008). Application of solid ash based catalysts in heterogeneous catalysis, *Environmental Science and Technology*, 42, pp. 7055–7063.
- [26] Wang, S., Ma, Q. & Zhu, Z.H. (2008). Characteristics of coal fly ash and adsorption application, *Fuel*, 87, pp. 3469–3473.

- [27] Wei, L., Wang, K., Zhao, Q., Xie, C., Qiu, W. & Jia, T. (2011). Kinetics and equilibrium of adsorption of dissolved organic matter fractions from secondary effluent by fly ash, *Journal of Environmental Sciences*, 23, pp. 1057–1065.
- [28] Yue, X., Duan, W., Lu, Y., Zhang, F. & Zhang, R. (2011). Effect of ZnO loading technique on textural characteristic and methyl blue removal capacity of exfoliated graphite/ZnO composites, *Bulletin of Materials Science*, 34, pp. 1569–1573.
- [29] Zhang, F., Zhao, Z., Tan, R., Guo, Y., Cao, L., Chen, L., Li, J., Xu, W., Yang, Y. & Song, W. (2012). Selective and effective adsorption of methyl blue by barium phosphate nano-flake, *Journal of Colloid Interface Science*, 386, pp. 277–284.